Journal of
Ceramic Science
and Technology

Synthesis, Densification and Characterization of Nanosized Oxide Ceramic Powders with Eutectic Compositions by Heating of Alcohol-Aqueous Salt Solutions

J.-H. Ouyang[*], Y.-H. Ma, A. Henniche, B. Wang, Z.-G. Wang, Y.-J. Wang

School of Materials Science and Engineering, Harbin
Institute of Technology, 92 Westdazhi Street, Harbin 150001, China

Abstract

Nanosized spherical powders of Al_2O_3-ZrO_2 (Y_2O_3) and Al_2O_3-$SmAlO_3$ with eutectic compositions have been synthesized with a facile and novel method involving the heating of aqueous salt solutions with an alcohol-water mixture as the solvent. The kind and concentration of aqueous salt solutions have a significant influence on the precipitation and morphologies of the resulting powders. Nanoscale particulates with a narrow size distribution were successfully obtained. The amorphous powders are crystallized to a mixture of t-ZrO_2 phase and α-Al_2O_3 phase at a calcination temperature of 1250 °C. Al_2O_3-ZrO_2 (Y_2O_3) powders exhibit an average particle size of 200 nm after calcination. However, fine Al_2O_3-$SmAlO_3$ nano-powders with an average size of 40 nm were synthesized after calcination at 1300 °C in which the resulting precipitates are crystallized to a mixture of α-Al_2O_3 and orthorhombic $SmAlO_3$. These ceramic powders were densified by hot pressing to further evaluate their microstructure and mechanical properties. The as-sintered Al_2O_3-ZrO_2 (Y_2O_3) ceramic consists of 42.8 wt% t-ZrO_2 and 57.2 wt% α-Al_2O_3 with a relative density of 98.5 %, and has a flexural strength of 1363 MPa and fracture toughness of 10.01 MPa·m$^{1/2}$, which is mainly attributed to phase transformation toughening of t-ZrO_2 to m-ZrO_2 during fracture. However, the Al_2O_3-$SmAlO_3$ ceramic has a relative density of 99.2 %, but flexural strength of just 529 MPa.

Keywords: Al_2O_3-ZrO_2(Y_2O_3) ceramic, Al_2O_3-$SmAlO_3$ ceramic, co-precipitation, microstructure morphology, mechanical properties

I. Introduction

High-performance oxide ceramics have attracted great attention for high-temperature structural applications and advanced manufacturing of hot-section components. The mechanical performance of oxide ceramics is dramatically influenced by grain size owing to a variety of size-dependent properties. A specific nano-structuration of oxide ceramics plays an important role in the improvement of their mechanical properties. Recently, Al_2O_3-based eutectic composites have been developed for ultra-high temperature applications as a substitute for superalloys, monolithic alumina and zirconia. A suitable percentage of zirconia in alumina-zirconia composites could significantly improve their fracture toughness [1-3]. The incorporation of some rare-earth oxides Ln_2O_3 (Ln = Eu, Gd, Dy, Ho, and Er) into such a composite can strengthen the grain boundary against mechanical creep at elevated temperatures [4]. The addition of Al_2O_3 nanoparticles to porous alumina increases its bending strength and fracture toughness [5,6]. Moreover, the infrared absorption, non-radiative relaxation, and heat transfer properties of Al_2O_3 ceramic are enhanced with the use of Al_2O_3 nanoparticles [7,8].

Al_2O_3/$GdAlO_3$ and Al_2O_3/$Y_3Al_5O_{12}$ (YAG) eutectic ceramics prepared with the modified Bridgeman method exhibit outstanding mechanical performance at elevated temperatures, demonstrating strength of 500 – 600 MPa and 300 – 400 MPa, respectively, from room temperature to close to their melting points [9-10]. The solidified Al_2O_3-$GdAlO_3$ ceramic consists of a three-dimensional continuous microstructure of entangled Al_2O_3 and $GdAlO_3$, which provides remarkable properties [9]. However, oxide eutectic ceramics are generally prepared with different directional solidification methods. For instance, the laser floating zone melting method was employed for fabricating Al_2O_3/$Er_3Al_5O_{12}$/ZrO_2 eutectic ceramics, where the growth rate influences the microstructure considerably. At a low growth rate, a geometric network structure mainly consists of Al_2O_3 and $Er_3Al_5O_{12}$ with ZrO_2 phase embedded in the formed network, while during solidification at a high growth rate, the eutectic ceramics exhibit an irregular interpenetrated microstructure of these three phases [11]. The electron beam floating zone melting method was also applied to fabricate Al_2O_3/YAG/YSZ eutectic ceramic with a Chinese script structure [12]. Recently, the induction heating zone melting method was used for the preparation of a Al_2O_3/$MgAl_2O_4$/ZrO_2 ternary eutectic ceramic. The eutectic rods consist of Al_2O_3, $MgAl_2O_4$

*   Corresponding author: ouyangjh@hit.edu.cn

phases as a matrix and ZrO_2 phase with a fiber or shuttle shape is embedded in the matrix [13]. Moreover, conventional methods such as explosion synthesis were used for fabricating Al_2O_3/ZrO_2 eutectic ceramic with a ZrO_2 phase embedded into the rod-like matrix of Al_2O_3 [14]. Although different methods are employed for preparing oxide eutectic ceramics as mentioned above, they still suffer from some limitations such as low fabrication efficiency and performance in that directionally solidified eutectics are only restricted to a simple cylindrical geometry and a limited sample size. In addition, the laser zone melting method is time-consuming for the fabrication of Al_2O_3-ZrO_2 (Y_2O_3) eutectic ceramics owing to the slow growth rate [15, 16] and high energy consumption in the case of laser-engineered net shaping [17]. Moreover, the Bridgman method generally results in large interphase spacings in oxide eutectics owing to a relatively low temperature gradient [18]. Whereas the cooling rate is limited by the magnitude of thermal gradient, which leads to the formation of a colony microstructure and high crack sensibility owing to high melting point and low fluidity as well as a complex processing procedure [19]. Hence, the large-scale production of crack-free bulk oxide ceramics with a fine and homogeneous eutectic microstructure by means of the above-mentioned conventional fabrication methods is very difficult.

It is necessary to develop a novel, simple and cost-effective method for the large-scale production of high-performance oxide eutectic ceramics. In the present work, nanosized spherical powders of Al_2O_3-ZrO_2(Y_2O_3) and Al_2O_3-$SmAlO_3$ with eutectic compositions are prepared with a cost-effective chemical co-precipitation method by carefully controlling the reaction conditions and the additives. Thereby, an effective and energy-saving method is needed for the large-scale production of homogeneous oxide composite nanopowders with eutectic compositions and high purity based on the mixing of different inexpensive precursors that are commercially available as starting materials. The chemical co-precipitation method is characterized as a rapid and simple manufacturing process with reproducible results at relatively low temperatures, which provides a molecular level of mixing and advantages for obtaining homogeneous and fine microstructures [20].

The phase structure, morphology and size of ceramic nanopowders were investigated in a calcination temperature range of 400 °C to 1300 °C. These ceramic powders were densified by means of hot pressing to further evaluate their microstructure and mechanical properties.

II. Experimental Procedure

The co-precipitation method was employed to fabricate Al_2O_3-ZrO_2 (3 mol% Y_2O_3) and Al_2O_3-$SmAlO_3$ nanopowders. In a typical synthesis approach, the solvent is a mixture of alcohol-aqueous salts solution with different alcohol-water ratios. The solution was heated and stirred during chemical co-precipitation. During heating, the dielectric constant of the alcohol-aqueous solution decreases significantly compared with that of the only aqueous solution as solvent. In this work, $Al(NO_3)_3$ $\cdot 9H_2O$ (Tianjin Fuchen Chemical Reagent Co. Ltd., Tianjin, China; Analytical), $ZrOCl_2 \cdot 8H_2O$ (Zibo Huantuo Chemical Co., Ltd., Zibo, China; Analytical), and rare-earth oxides of Y_2O_3 and Sm_2O_3 (Grirem Advanced Materials Co., Ltd., Beijing, China; ≥ 99.9 %) were used as starting materials for fabricating Al_2O_3-ZrO_2(Y_2O_3) and Al_2O_3-$SmAlO_3$ nanopowders with eutectic compositions based on the heating of alcohol-aqueous salt solutions. Different starting materials as mentioned above were weighed according to the eutectic composition as listed in Table 1. Sm_2O_3, $ZrOCl_2 \cdot 8H_2O$ and Y_2O_3 were dissolved in a minimum quantity of nitric acid, respectively, and maintained at 40 °C with continuous stirring. These solutions were then added to the aluminum-nitrate solution dissolved in an alcohol-water mixture separately with different isopropanol/water ratios and cation concentrations for the preparation of Al_2O_3-$SmAlO_3$ and Al_2O_3-ZrO_2(Y_2O_3) nanopowders, respectively. The mixed aqueous solutions were thoroughly stirred at room temperature, and a small amount of polyethylene glycol (PEG) was added as the surfactant to the solution. Meanwhile, urea and ammonia were used for precipitation in order to investigate their effects on the morphology and particle size of the prepared powders. The precipitates were obtained by careful tailoring of the reactions conditions and the amounts of urea and ammonia additives. After precipitation, the solutions were consolidated by means of a high-speed centrifugal casting machine (Xiangyi Centrifugal Machines Ltd., Changsha, China) at 8000 rpm for 2 h. After centrifugation, the supernatant was poured off, and replaced with distilled water and aged at room temperature. The operation was repeated until a pH value of 7 was reached. However, for Al_2O_3-ZrO_2(Y_2O_3) nanopowder, the slurry was washed repeatedly with distilled water and/or alcohol to remove chloride and nitrate ions, and was then filtered (as tested with $AgNO_3$ solution) maintaining a pH value of 7. The obtained slurries were aged with ethanol at room temperature, and then oven-dried at 60 °C for 2 – 5 h. The dried powders were ground into fine powder and calcined in air in a furnace at temperatures of 400 – 1300 °C for 2 h.

Table 1: Designed eutectic compositions of Al_2O_3-ZrO_2(Y_2O_3) and Al_2O_3-$SmAlO_3$ oxide ceramic powders (mol%).

Powder Materials	Al_2O_3-ZrO_2(Y_2O_3)		Al_2O_3-$SmAlO_3$	
	Al_2O_3	ZrO_2 (3mol.% Y_2O_3)	Al_2O_3	$SmAlO_3$
Eutectic compositions (mol%)	62	38	52	48

The co-precipitated powders were synthesized against agglomeration by carefully tailoring the reaction conditions, including the processing parameters of the ionic concentration, the alcohol/water molar ratio in the aqueous salt solution, calcination temperature and drying method to produce monodisperse and fine spherical particles. Therefore, in order to fabricate fully densified Al_2O_3-$ZrO_2(Y_2O_3)$ and Al_2O_3-$SmAlO_3$ ceramics with eutectic compositions, the synthesized powders free of agglomeration were sintered by means of the hot-pressing technique. Firstly, the powders were cold-compacted in a graphite die with a pressure of 30 MPa, and then sintered in a hot-pressing furnace (Advanced Vacuum System, AVS-2200, AVS Inc., USA) for 1 h in vacuum at temperatures of 1400, 1500 and 1600 °C, respectively, with a heating rate of 20 °K/min and an applied pressure of 30 MPa. An X-ray diffractometer (XRD, Rigaku D/Max-γB, Japan) was used to identify the phase structures present in the precursors, the crystalline powders after calcination and the sintered bulks with monochromatic CuKα radiation in a 2θ range of 10 – 90°. The measurements were performed at a scan rate of 4° min^{-1} with a step size of 0.02°. The morphology and size of the ceramic powders and the microstructure of the as-sintered ceramic bulks were observed with field-emission scanning electron microscope (FESEM, FEI Helios Nanolab600i, USA). A transmission electron microscope (TEM, FEI Tecnai G2F30, USA) equipped with Energy-Dispersive X-ray Spectroscopy (EDS) was employed for morphology observations and element composition analysis of ultrafine particles.

Specimens for the mechanical tests were machined into rectangular bar shapes with dimensions of 3 mm × 4 mm × 36 mm for strength tests and 2 mm × 4 mm × 20 mm for fracture toughness tests, respectively. The flexural strength in a three-point configuration with a span of 30 mm was tested at room temperature, using a crosshead speed of 0.5 mm/min. Fracture toughness was measured with the single-edge-notch beam (SENB) method, using a crosshead speed of 0.05 mm/min. All of these tests at room temperature were conducted on a universal testing machine (Instron 5569, USA). The high-temperature flexural strength of ceramic bulks was tested at 1000 °C in a three-point bending tester (Instron-5500R universe tester, USA). Before the tests, the specimens were polished to a mirror finish, and the edges of the specimens were beveled to prevent fracturing from edge cracks. Density of the specimens was measured according to the Archimedes principle. A Vickers hardness tester (HVS-30 type) was used to evaluate the hardness of ceramic bulks under the loading condition of 294 N for 15 s. At least seven specimens were tested for each experiment.

III. Results and Discussion

(1) Powder synthesis and characterization

The phase transitions of the powder precursors are investigated at different calcination temperatures of 400 – 1300 °C for 2 h in order to synthesize both Al_2O_3-ZrO_2 (Y_2O_3) and Al_2O_3-$SmAlO_3$ ceramic nanopowders with eutectic compositions by using urea and ammonia as the precipitants, respectively. According to the

XRD patterns as shown in Fig. 1, the precursors and fine powders demonstrate a complete crystallization of different ceramic oxides of ZrO_2 and $SmAlO_3$ comparative to α-Al_2O_3 after calcination. Therefore, in the case of Al_2O_3-$ZrO_2(Y_2O_3)$ powders, no peaks of α-Al_2O_3 are observed at low calcination temperatures. Meanwhile, peaks of t-ZrO_2 crystal phase are observed after calcination at temperatures up to 800 °C as demonstrated in Fig. 1(a). Moreover, further increasing the calcination temperature leads to crystallization of the α-Al_2O_3 phase, and the corresponding peaks of α-Al_2O_3 phase are clearly observed at 1250 °C. Likewise, in the case of Al_2O_3-$SmAlO_3$ powders, intense and acute peaks of $SmAlO_3$ phase are observed after calcination at 1100 °C showing good crystallization. However, the calcination temperature corresponding to the crystallization of α-Al_2O_3 phase is 1300 °C, in which α-Al_2O_3 peaks are identified in the XRD patterns as shown in Fig. 1(b).
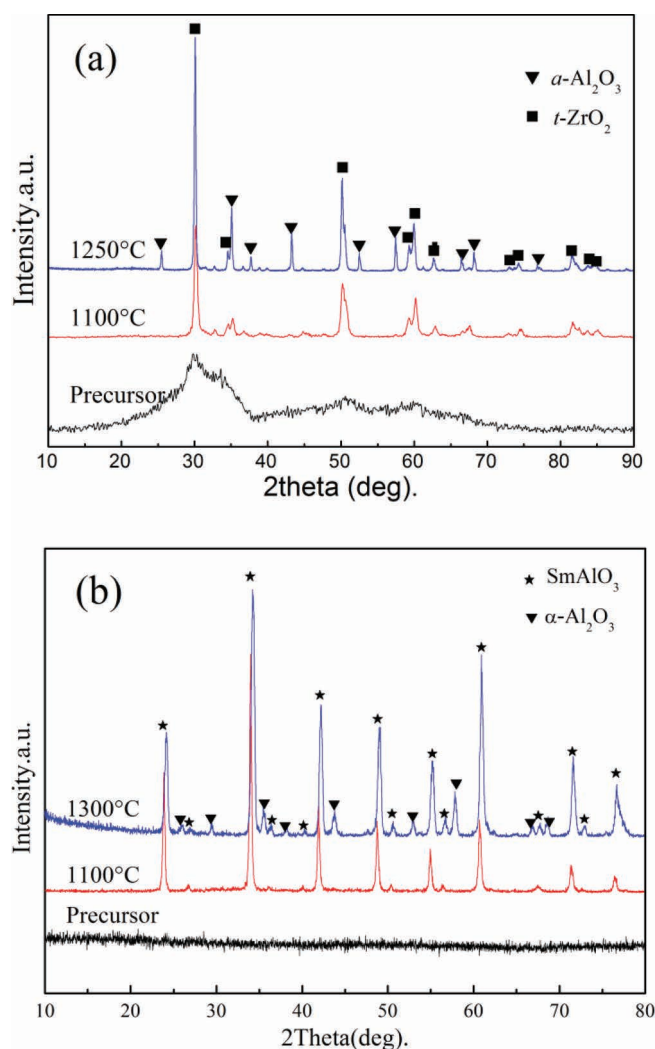

Fig. 1: X-ray diffraction patterns of Al_2O_3-$ZrO_2(Y_2O_3)$ and Al_2O_3-$SmAlO_3$ ceramic powders before and after calcination at different temperatures: (a) Al_2O_3-$ZrO_2(Y_2O_3)$; (b) Al_2O_3-$SmAlO_3$.

Morphology and size of the precursors and the calcined ceramic powders are investigated using SEM observations. Fig. 2 shows SEM micrographs of powder precursors obtained by using different precipitation agents with a
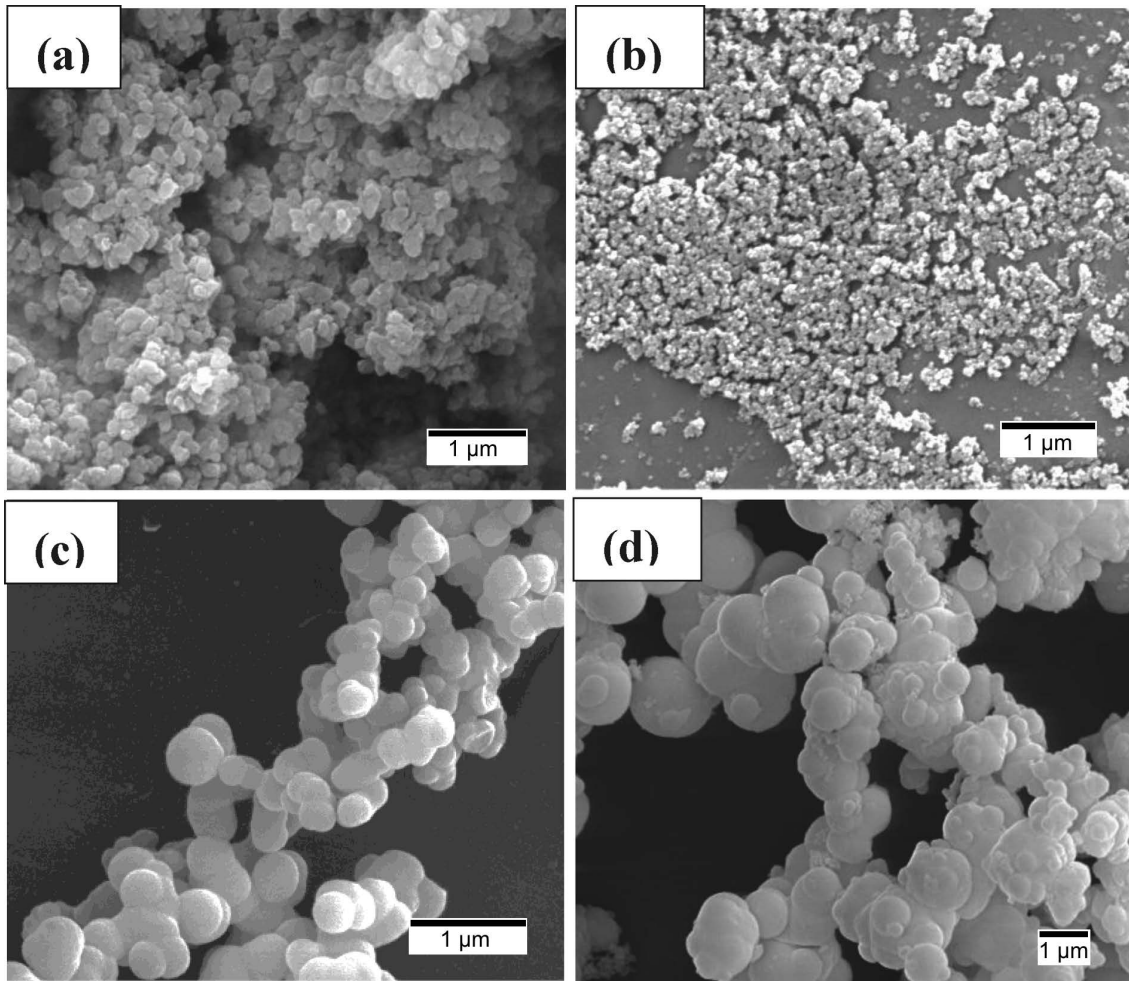
Fig. 2: SEM micrographs of different powder precursors: (a) Al_2O_3-$ZrO_2(Y_2O_3)$ precursors with ammonia as the precipitant; (b) Al_2O_3-$SmAlO_3$ precursors with ammonia as the precipitant; (c) Al_2O_3-$ZrO_2(Y_2O_3)$ precursors with urea as the precipitant; (d) Al_2O_3-$SmAlO_3$ precursors with urea as the precipitant.

mixture of isopropanol and water in a ratio of 3:1. Indeed, the powder precursors of Al_2O_3-$ZrO_2(Y_2O_3)$ exhibit high homogeneity, good dispersion and fair particle size on all the micrographs. In contrast to Al_2O_3-ZrO_2 (Y_2O_3) powders, the Al_2O_3-$SmAlO_3$ powder precursor exhibits a smaller particle size of about 50 – 100 nm, as shown in Fig. 2(b), using ammonia as a precipitation agent. However, in both synthesized powder precursors an irregular spherical shape has been formed. In the case of urea as the precipitant instead of ammonia, the synthesis process takes a long reaction time of 10 to 20 h owing to the slow reaction between urea and water as required for nucleation and spontaneous precipitation under heating at 90 °C. The reaction is described as follows:

$$CO(NH_2)_2 + 3H_2O \rightarrow CO_2 + 2NH_2^+ + 2OH^- \qquad (1)$$

As the above-mentioned reaction leads to a homogeneous hydroxide distribution, the synthesized precursor consists of spherical primary particles with high homogeneity. However, the powder precursors exhibit a larger particle size than those when ammonia is used as the precipitant in which Al_2O_3-ZrO_2 (Y_2O_3) powder precursor shows a range of 300 – 400 nm particle size. Meanwhile, Al_2O_3-$SmAlO_3$ powder precursor is in the scale of micrometers. From SEM observations of different powder precursors, ammonia is suitable for the synthesis of

Al_2O_3-$SmAlO_3$ nanoscale powders, while urea is more convenient for use in the preparation of Al_2O_3-ZrO_2 (Y_2O_3) powders.

The powder morphology is closed related to the physical properties of the liquid media, which influences the agglomeration of Al_2O_3-ZrO_2 (Y_2O_3) powder precursor during the precipitation process. The energy barrier V_b that prevents the agglomeration between two particles can be expressed in two parts [21]. The first part is the van der Waals attraction, which remains constant under different reaction conditions, while the second part is known as the electrostatic repulsion of particles, which determines the magnitude of V_b (eV) written as the following:

$$V_b = \frac{-A \cdot k \cdot \alpha}{12} + 2\pi \cdot \varepsilon_0 \cdot \varepsilon_r \cdot \Psi^2 \qquad (2)$$

where A is the effective Hamaker constant, k is the Debye-Hückel parameter, α is the particle diameter, ε_r is the dielectric constant of the liquid medium, ε_0 is the permittivity of vacuum, and Ψ is the surface potential. The Debye-Hückel parameter k can be expressed as follows:

$$k = \left(\frac{2F^2Z^2N_0}{\varepsilon_0\varepsilon_r k_b T}\right)^{1/2} \qquad (3)$$

where k_b is the Boltzmann constant, F is the Faraday constant, T is the absolute temperature, Z is the ionic valence and N_0 is the concentration of the electrolyte.

The constituents of liquid media are optimized to be a mixture of isopropanol/water with a specific ratio in order to increase the energy barrier V_b and introduce the required repulsion. Indeed, primary particles precipitated from this solution are spherical in shape, and exhibit a high energy barrier against coagulation, as demonstrated in Fig. 3.
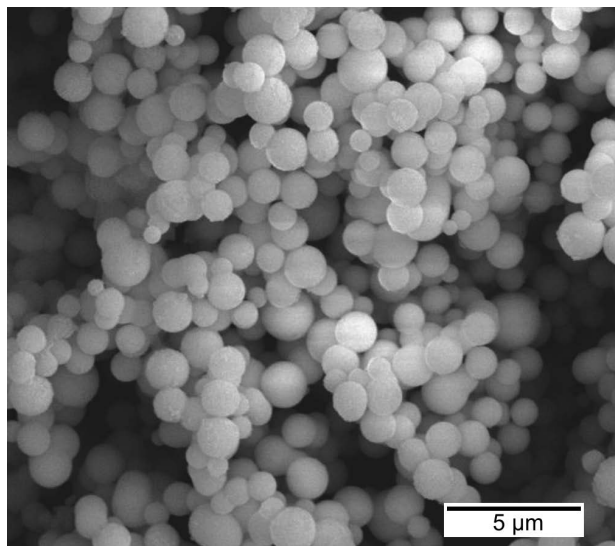

Fig. 3: SEM images of Al_2O_3/ZrO_2 (Y_2O_3) powder precursors by heating isopropanol/water (3:1) salt solutions.

Al_2O_3-ZrO_2(Y_2O_3) powder precursors via chemical co-precipitation followed by various drying methods are shown in Fig. 4. By means of direct microscopic observations from SEM images, the degree of agglomeration and the shape of the co-precipitated powders were determined with very little residual uncertainty. As seen clearly from the SEM images showing the appearance of the powders, the morphologies of oxide powders are substantially affected by the drying methods employed. The resulting powders from different drying methods exhibit high homogeneity and are spherical in shape. However, the powders prepared by means of only water washing are dramatically agglomerated. In contrast, alcohol washing followed by oven/microwave drying produces high-dispersion and fine spherical nanoparticles, which show an advantage over freeze drying and azeotropic distillation, respectively. Likewise, the effects of the isopropanol/water ratio and cations concentration on the synthesis of Al_2O_3-$SmAlO_3$ powder precursor. Fig. 5 shows the micrographs of Al_2O_3-$SmAlO_3$ powder precursors at different cation concentrations and the isopropanol/water ratio of 3:2. Hence, the liquid media followed by different drying methods has considerable effects on the dispersion and particle morphologies. Fine Al_2O_3-$SmAlO_3$ powders with a spherical shape are obtained in the alcohol-aqueous salt solution with the isopropanol/water ratio of 3:2 and the cation concentration of 0.1 mol/L.
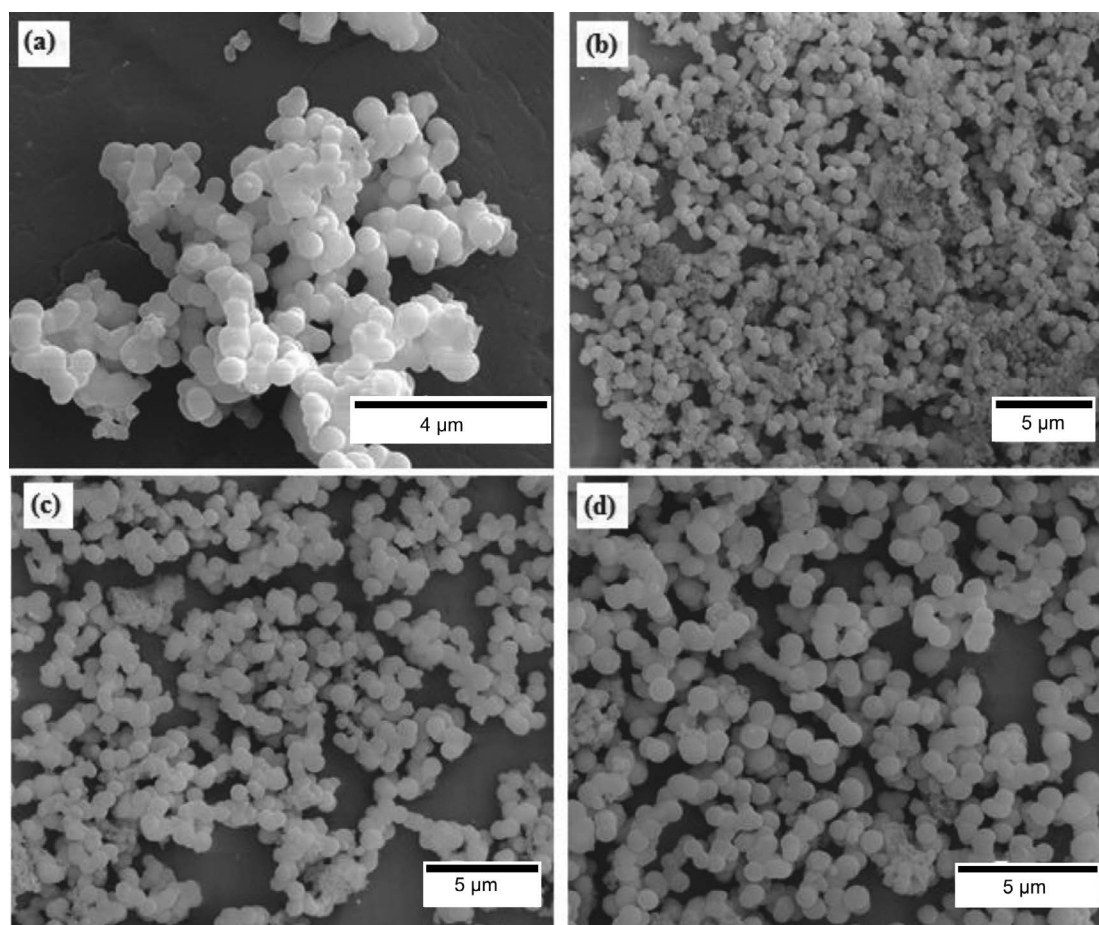

Fig. 4: SEM images of Al_2O_3/ZrO_2(Y_2O_3) powder precursors after washing followed by different drying methods: (a) water washing and drying; (b) alcohol washing and drying; (c) freeze drying; (d) azeotropic distillation.
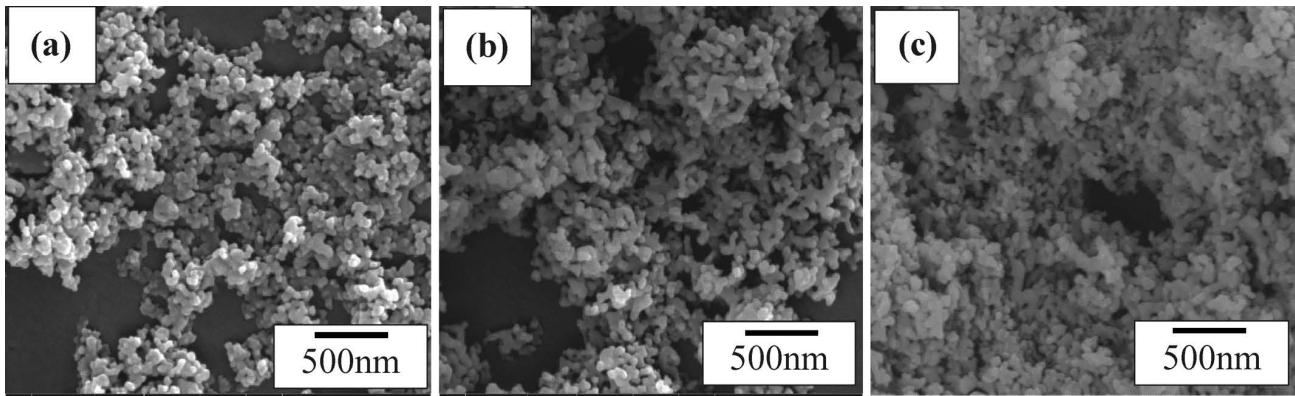
Fig. 5: SEM images of Al_2O_3-$SmAlO_3$ precursors synthesized at different cation concentrations: (a) 0.05 mol/L; (b) 0.1 mol/L; and (c) 0.2 mol/L.

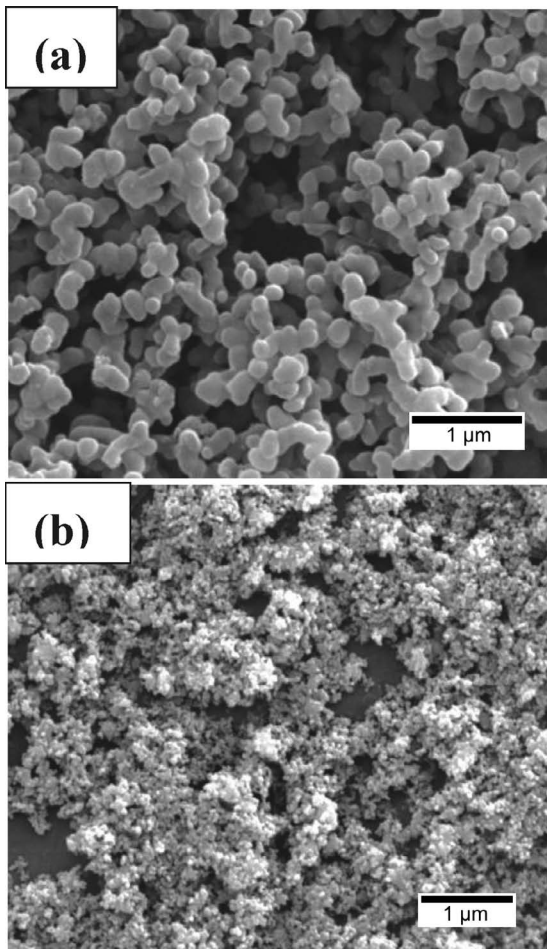**Fig. 6:** SEM images of oxide ceramic powders after calcination: (a) Al_2O_3-$ZrO_2(Y_2O_3)$ powder with urea as the precipitant after calcination at 1250 °C; (b) Al_2O_3-$SmAlO_3$ powder with ammonia as the precipitant after calcination at 1300 °C.

The difference in the morphology of the co-precipitated powders can be explained by a high-energy barrier of V_b as presented in Eq. (2), which produces small particles that are weakly agglomerated as the energy barrier between particles depends mostly upon the decrease in the dielectric constant. The dielectric constant of an alcohol-water solvent mixture decreases with increasing volume ratio of alcohol to water [22].

Fig. 6 shows the SEM morphologies of Al_2O_3-ZrO_2 (Y_2O_3) and Al_2O_3-$SmAlO_3$ powder precursors pre-

pared by ammonia calcined at temperatures of 1250 °C and 1300 °C, respectively. From Fig. 6, both Al_2O_3-ZrO_2 (Y_2O_3) and Al_2O_3-$SmAlO_3$ powders are in high dispersion, and exhibit an irregular spherical shape after calcination. Al_2O_3-$ZrO_2(Y_2O_3)$ powder has a larger particle size than Al_2O_3-$SmAlO_3$ powder, in addition to small agglomeration in some degree resulting from the partial sintering after calcination.

(2) Bulk consolidation and mechanical properties

The Al_2O_3-$ZrO_2(Y_2O_3)$ nanopowders after calcination at 1250 °C were hot-pressed in vacuum for 1 h with an applied pressure of 30 MPa at temperatures of 1400, 1500 and 1600 °C, respectively, with a heating rate of 20 °K/min to fabricate dense ceramic bulks. The as-sintered ceramic bulks are devoid of macroscopic defects such as pores and cracks. Indeed, Al_2O_3-$ZrO_2(Y_2O_3)$ ceramic exhibits a high relative density, which increases with increasing sintering temperature from 1400 to 1600 °C. Fig. 7 shows the XRD patterns of Al_2O_3-ZrO_2 (Y_2O_3) ceramics hot-pressed at different temperatures. The phases present consist mainly of α-Al_2O_3 and t-ZrO_2 phases in addition to weak peaks corresponding to a small amount of m-ZrO_2 owing to the stabilizing function of Y_2O_3. The high content of alumina inhibits effectively the nucleation and grain growth of metastable t-ZrO_2 as reported previously [23].
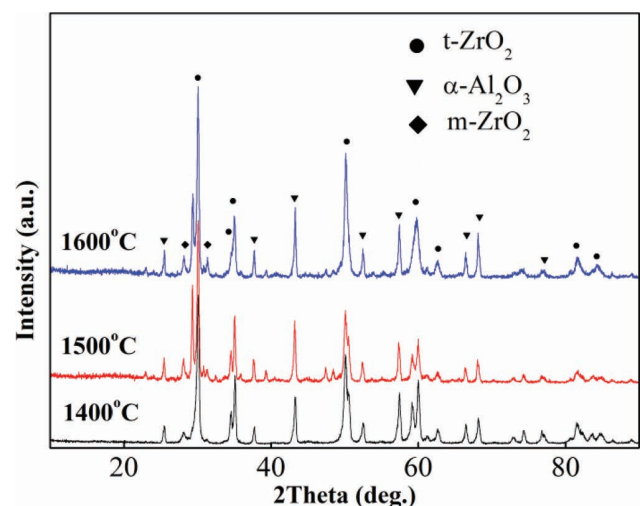

Fig. 7: X-ray diffraction patterns of Al_2O_3-$ZrO_2(Y_2O_3)$ ceramics sintered at different temperatures.
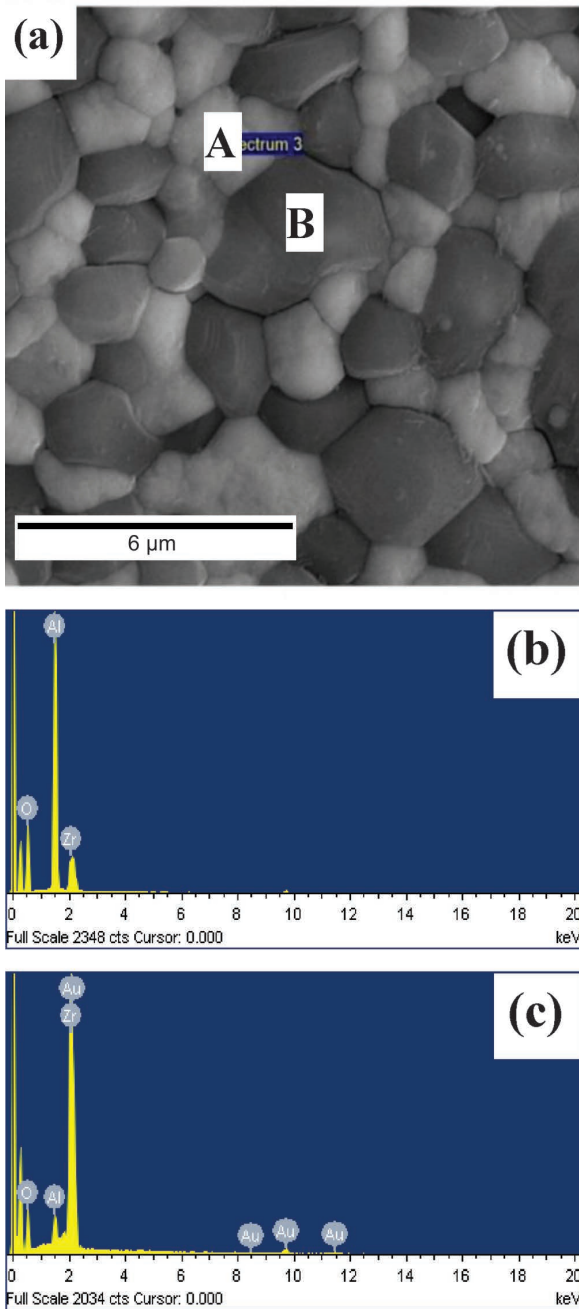
Fig. 8: SEM micrograph and EDS analysis of Al_2O_3-$ZrO_2(Y_2O_3)$ ceramic sintered at 1500 °C: (a) microstructure; (b) EDS analysis of the position B; (c) EDS analysis of the position A.

Fig. 8 shows a SEM micrograph and EDS analysis of Al_2O_3-$ZrO_2(Y_2O_3)$ ceramic sintered at 1500 °C. The Al_2O_3-$ZrO_2(Y_2O_3)$ ceramic consists of two different regions, according to EDS analysis, the dark region is identified as α-Al_2O_3, while the bright region is identified as t-ZrO_2, in addition to some t-ZrO_2 nanosized grains in the interior of α-Al_2O_3, as shown in Fig. 9. t-ZrO_2 grains exhibit a smaller average size than α-Al_2O_3 grains. The phase constituents of Al_2O_3-$ZrO_2(Y_2O_3)$ ceramic sintered at 1500 °C are measured using the Image Pro-Plus Software. As shown in Fig. 10, the phase composition is identified to be 57.2 wt% Al_2O_3 and 42.8 wt% ZrO_2.

Table 2 shows the mechanical properties of the Al_2O_3-$ZrO_2(Y_2O_3)$ ceramics hot-pressed at 1500 °C for 1 h. The Al_2O_3-$ZrO_2(Y_2O_3)$ ceramic exhibits a relative den-

sity of 98.5 %, a room-temperature flexural strength of 1363 MPa, a Vickers hardness of 16.8 GPa and a high-temperature flexural strength of 371 MPa at 1000 °C. The measured fracture toughness of 10.01 MPa·$m^{1/2}$ in this work is clearly higher than those of Al_2O_3-$ZrO_2(Y_2O_3)$ eutectic ceramics fabricated by means of laser-engineered net shaping (4.79 MPa $m^{1/2}$) [17] and spark plasma sintering (7.4 MPa $m^{1/2}$) [24], respectively. The high fracture toughness and mechanical strength of Al_2O_3-$ZrO_2(Y_2O_3)$ ceramics is attributed to phase alternation and the fine microstructure established after sintering of nanopowders synthesized by means of chemical co-precipitation.
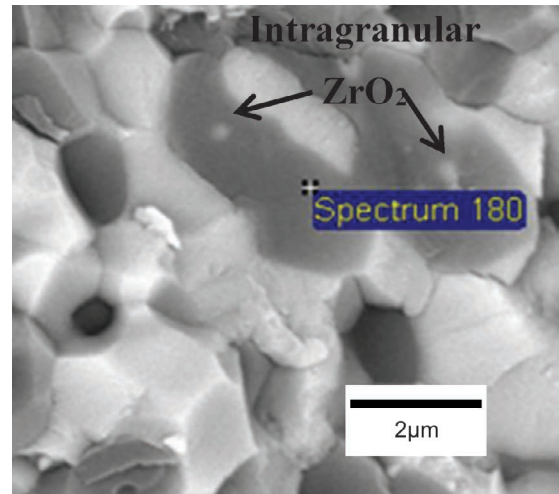

Fig. 9: SEM micrograph showing some intragranular ZrO_2 dispersed in α-Al_2O_3 grains.

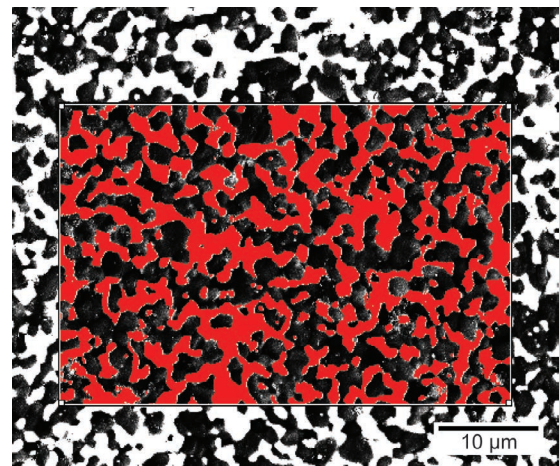Fig. 10: Phase composition analysis of the as-sintered Al_2O_3-$ZrO_2(Y_2O_3)$ ceramic sintered at 1500 °C.

Fig. 11 shows X-ray diffraction patterns of Al_2O_3-ZrO_2 (Y_2O_3) ceramic sintered at 1500 °C before and after bending tests at room temperature. The Al_2O_3-ZrO_2 (Y_2O_3) ceramic after bending tests at room temperature consists mainly of α-Al_2O_3, m-ZrO_2, a small amount of t-ZrO_2 and $Zr_3Y_4O_{12}$ phases. From XRD analysis of Al_2O_3-$ZrO_2(Y_2O_3)$ ceramic performed after fracture, strong m-ZrO_2 peaks are identified clearly, as shown in Fig. 11, which are attributed to the phase transformation of t-ZrO_2 to m-ZrO_2 induced by the crack propagation and fracture during bending tests.
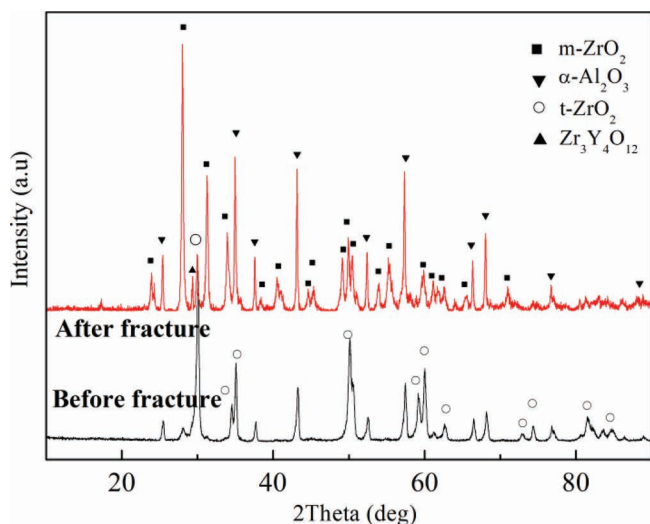
Fig. 11: X-ray diffraction patterns of Al_2O_3-$ZrO_2(Y_2O_3)$ ceramic sintered at 1500 °C before and after fracture.

The Al_2O_3-$SmAlO_3$ powders after calcination at 1300 °C were hot-pressed in vacuum for 1 h with an applied pressure of 30 MPa at temperatures of 1400, 1500 and 1600 °C, respectively, with a heating rate of 20 °K/min to fabricate dense ceramic bulks. The Al_2O_3-$SmAlO_3$ ceramic is free of defects, and exhibits a high relative density. According to the XRD patterns shown in Fig. 12, Al_2O_3-$SmAlO_3$ ceramic is composed of $SmAlO_3$ and α-Al_2O_3 phase, and no other phase is identified in the XRD patterns. The microstructure of Al_2O_3-$SmAlO_3$ ceramic sintered at different temperatures is shown in Fig. 13. Clearly, the Al_2O_3-$SmAlO_3$ ceramic has a fine microstructure and a homogeneous phase distribution consisting of both dark α-Al_2O_3 and bright $SmAlO_3$ regions as identified from the EDS analysis in Fig. 13(d). The Al_2O_3-$SmAlO_3$ ceramic sintered at 1500 °C has a relative density of 99.2 %, a room-temperature flexural strength of 529 MPa, a fracture toughness of 5.50 MPa·m$^{1/2}$, a Vickers hardness of 15.6 GPa, and high-temperature flexural strength of 318 MPa after testing at 1000 °C, as shown in Table 2.

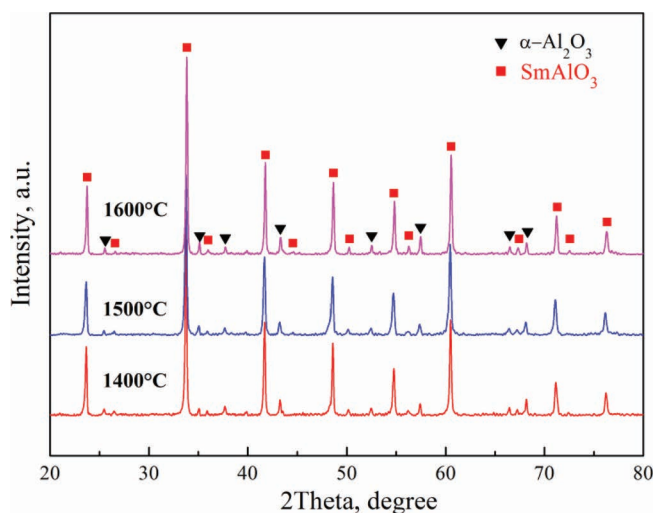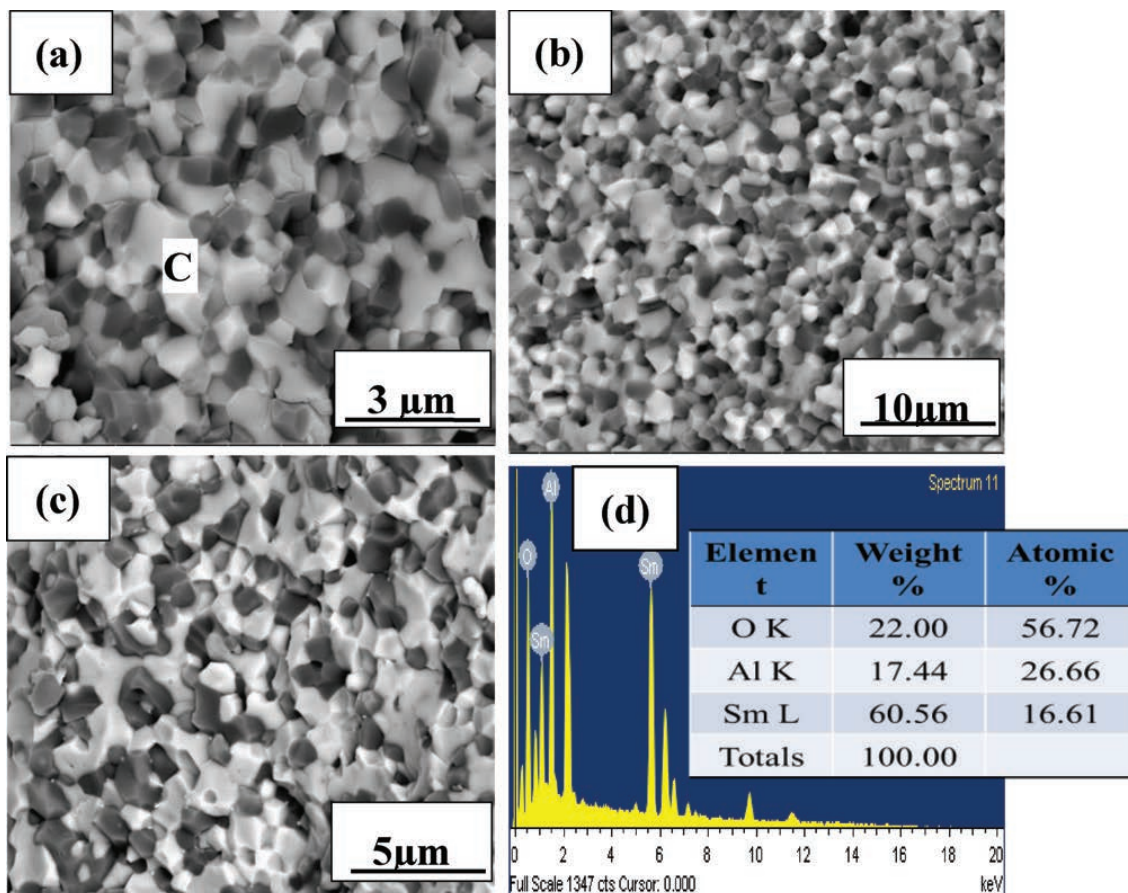**Fig. 12:** X-ray diffraction patterns of Al_2O_3-$SmAlO_3$ samples hot-pressed at different temperatures.

Fig. 13: Microstructure and EDS analysis of Al_2O_3-$SmAlO_3$ samples hot-pressed at different temperatures: (a) at 1400 °C; (b) at 1500 °C; (c) 1600 °C; (d) EDS analysis of the position C in (a).

Table 2: Mechanical properties of the as-sintered Al_2O_3-$ZrO_2(Y_2O_3)$ and Al_2O_3-$SmAlO_3$ ceramics with eutectic composition hot-pressed at 1500 °C.

As-sintered Ceramics	Relative density (%)	Flexural strength (MPa)	Flexural strength (MPa) at 1000 °C	Vickers hardness (GPa)	Fracture toughness MPa m$^{1/2}$
Al_2O_3-$ZrO_2(Y_2O_3)$	98.5 %	1363±28	371±16	16.8±0.4	10.01±0.8
Al_2O_3-$SmAlO_3$	99.2 %	529±14	318±20	15.6±0.2	5.50±0.3

IV. Conclusions

(1) Nanosized spherical Al_2O_3-$ZrO_2(Y_2O_3)$ and Al_2O_3-$SmAlO_3$ oxide powders with eutectic compositions have been successfully prepared by means of heating of aqueous salt solutions with an alcohol-water mixture as the solvent.

(2) In the case of using zirconyl chloride and yttrium- or aluminum-nitrate solutions as the reactant solutions, the resulting nanoscale particulates have a narrow size distribution in which these amorphous powders are crystallized to a mixture of t-ZrO_2 phase and α-Al_2O_3 phase at 1250 °C. However, when aluminum-nitrate, samarium-nitrate solutions are employed as the reaction species, the resulting precipitates are crystallized to a mixture of α-Al_2O_3 and orthorhombic $SmAlO_3$ at 1300 °C. After calcination, these ceramic powders have a particle size of 40 to 200 nm.

(3) Hot pressing is employed to fabricate fully densified Al_2O_3-$ZrO_2(Y_2O_3)$ and Al_2O_3-$SmAlO_3$ ceramics with eutectic compositions. The as-sintered Al_2O_3-ZrO_2 (Y_2O_3) ceramic consists of 42.8 wt% t-ZrO_2 and 57.2 wt% α-Al_2O_3. The Al_2O_3-ZrO_2 (Y_2O_3) ceramic has a relative density of 98.5 %, a room-temperature flexural strength of 1363 MPa, a fracture toughness of 10.01 MPa·m$^{1/2}$ and a high-temperature flexural strength of 371 MPa at 1000 °C. However, the Al_2O_3-$SmAlO_3$ ceramic has a relative density of 99.2 %, but only room-temperature flexural strength of 529 MPa, a fracture toughness of 5.50 MPa·m$^{1/2}$ and high-temperature flexural strength of 318 MPa at 1000 °C.

Acknowledgements

References

[1] Aza, A.H., Chevalier, J., Fantozzi, G.: Slow crack growth behavior of zirconia-toughened alumina ceramics processed by different methods, *J. Am. Ceram. Soc.*, **86**, 115–120, (2003).

[2] Chevalier, J.: What future for zirconia as a biomaterial, J. *Biomaterials*, **27**, 535–543, (2006).

[3] Buban, J.P., Chen, K.J., Shibata, N., Ching, W.Y., Yamamoto, T., Ikuhara, Y.: Grain boundary strengthening in alumina by rare earth impurities, *J. Science.*, **311**, 212–215, (2006).

[4] Li, T., Chen, Q., Schadler, L.S., Siegel, R.W.: Scratch behavior of nanoparticle Al_2O_3-filled gelatin films, *J. Polymer Composites.*, **23**, 1076–1086, (2002).

[5] Ogawa, K., Vogt, T., Ullmann, M., Johnson, S., Friedlander, S.K.: Elastic properties of nanoparticle chain aggregates of TiO_2, Al_2O_3, and Fe_2O_3 generated by laser ablation, *J. Appl. Phys.*, **87**, 63–73, (2000).

[6] Li, G., Jiang, Z., Jiang, A., Zhang, L.: Strengthening of porous Al_2O_3 ceramics through nanoparticle addition, *J. Nanostruct. Mater.*, **8**, 749–754, (1997)

[7] Shek, C.H., Lai, J.K.L., Gu, T.S., Lin, G.M.: Transformation evolution and infrared absorption spectra of amorphous and crystalline nano-Al_2O_3 powders, *J. Nanostruct. Mater.*, **8**, 605–610, (1997).

[8] Maïga, S.B., Nguyen, C.T., Galanis, N., Roy, G., Maré, T., Coqueux, M.: Heat transfer enhancement in turbulent tube flow using Al_2O_3 nanoparticle suspension, *Int. J. Numer. Method H.*, **16**, 275–292, (2006).

[9] Waku, Y., Nakagawa, N., Wakamoto, T., Ohtsubo, H., Shimizu, K., Kohtoku, Y.: Ductile ceramic eutectic composite with high strength at 1873 K, *J. Nature.*, **389**, 49–52, (1997).

[10] Waku, Y. Sakata, S., Mitani, A., Shimizu, K.: Temperature dependence of flexural strength and microstructure of $Al_2O_3/Y_3Al_5O_{12}/ZrO_2$ ternary melt growth composites, *J. Mater. Sci.*, **37**, 2975–2982, (2002).

[11] Mesa, M.C., Oliete, P.B., Pastor, J.Y., Martin, A. LLorca. J.: Mechanical properties up to 1900 K of $Al_2O_3/Er_3Al_5O_{12}/ZrO_2$ eutectic ceramics grown by the laser floating zone method, *J. Eur. Ceram. Soc.*, **34**, 2081–2087, (2014).

[12] Su, H.J., Zhang, J., Liu, L., Fu, H.Z.: Preparation and microstructure evolution of directionally solidified $Al_2O_3/YAG/YSZ$ ternary eutectic ceramics by a modified electron beam floating zone melting, *J. Mater. Lett.*, **91**, 92–95, (2013)

[13] Zhai, S., Liu, J., Wang, J.: Microstructure of the directionally solidified ternary eutectic ceramic $Al_2O_3/MgAl_2O_4/ZrO_2$, *J. Ceram Int.*, **42**, 8079–8084, (2016)

[14] Zheng, Y.T., Li, H.B., Zhou, T., Zhao, J., Yang, P.: Microstructure and mechanical properties of Al_2O_3/ZrO_2 eutectic ceramic composites prepared by explosion synthesis, *J. Alloy. Compd.*, **551**, 475–480, (2013).

[15] Larrea, A., De la Fuente, G.F., Merino, R.I., Orera, V.M.: ZrO_2-Al_2O_3 eutectic plates produced by laser zone melting, *J. Eur. Ceram. Soc.*, **22**, 191–198, (2002).

[16] Larrea, A., Orera, V.M., Merino, R.I., Pena, J.I.: Microstructure and mechanical properties of Al_2O_3-YSZ and Al_2O_3-YAG directionally solidified eutectic plates, *J. Eur. Ceram. Soc.*, **25**, 1419–1429, (2005).

[17] Niu, F., Wu, D., Ma, G., Wang, J., Guo, M., Zhang, B.: Nanosized microstructure of Al_2O_3-ZrO_2 (Y_2O_3) eutectics fabricated by laser engineered net shaping, *Scr. Mater.*, **95**, 39–41, (2015).

[18] Yao, B., Su, H., Zhang, J., Ren, Q., Ma, W., Liu, L., Fu, H.: Sintering densification and microstructure formation of bulk Al_2O_3/YAG eutectic ceramics by hot pressing based on fine eutectic structure, *Mater. Des.*, **92**, 213–222, (2016).

[19] Benamara, O., Lebbou, K.: Shaped ceramic eutectic plates grown from the melt and their properties, *J. Cryst. Growth*, **449**, 67–74, (2016).

[20] Hassanzadeh-Tabrizi, S.A., Mazaheri, M., Aminzare, M., Sadrnezhaad, S.K.: Reverse precipitation synthesis and characterization of CeO_2 nanopowder, *J. Alloy. Compd.*, **491,** 499 – 502, (2010).

[21] Hunter, R.J.: Foundations of colloid science, *Clarendon Press*, Oxford, UK, **1,** 443, (1987).

[22] Moon, Y.T., Park, H.K., Kim, D.K., Kim, C.H.: Preparation of monodisperse and spherical zirconia powders by heating of alcohol-aqueous salt solutions, *J. Am. Ceram. Soc.*, **78,** 2690 – 2694, (1995).

[23] Barrera, A., Fuentes, S., Viniegra, M., Avalos-Borja, M., Bogdanchikova, N., Campa-Molina, J.: Structural properties of Al_2O_3-La_2O_3 binary oxides prepared by sol-gel, *J. Mater. Res. Bull.*, **42,** 640 – 648, (2007).

[24] Xia, X., Li, X., Zhang, M., Zheng, D.: Transitional/eutectic microstructure of Al_2O_3-ZrO_2 (Y_2O_3) ceramics prepared by spark plasma sintering; *Mater. Lett.*, **175,** 212 – 214, (2016).